Author Manuscript

Color-stable, all-phosphorescent white organic light emitting diodes using the polariton-enhanced Purcell effect

Claire E. Arneson[1], Haonan Zhao[1], and Stephen R. Forrest[1,2,3,4,*]

[1] Department of Physics, University of Michigan, Ann Arbor, MI, 48109, USA

[2]Applied Physics Program, University of Michigan, Ann Arbor, MI, 48109, USA

[3]Department of Electrical Engineering and Computer Science, University of Michigan, Ann Arbor, MI, 48109, USA

[4]Department of Materials Science and Engineering, University of Michigan, Ann Arbor, MI, 48109, USA

Abstract

The short operational lifetimes of high efficiency phosphorescent organic blue light emitting devices (PHOLEDs) has long been a limiting factor in their use in displays and lighting. Previously, this problem has been avoided by using less efficient fluorescent blue devices in separately biased red, green, and blue emissive elements to achieve stable full color emission. However, the operational lifetime of blue phosphorescent OLEDs has been significantly improved through utilization of the plasmon-exciton-polariton-enhanced (PEP) Purcell effect. In this work, we demonstrate a white emitting PHOLED comprising stacked red, green, and blue elements that exploits PEPs to extend the operational lifetime of the blue element such that all color emissive layers degrade at the same rate. The device features white light emission with an external quantum efficiency of 19.1 ± 0.4%, a luminous power efficiency of 13.3 ± 0.3 lm/W at a luminance of 1000 cd m^{-2} when measured over 4π solid angle, with a color rendering index of 76 that is constant throughout the device aging to 70% of its initial luminance, T_{70}. We achieve 2.9 times

This is the author manuscript accepted for publication and has undergone full peer review but has not been through the copyediting, typesetting, pagination and proofreading process, which may lead to differences between this version and the Version of Record. Please cite this article as doi: 10.1002/adfm.202410741.

This article is protected by copyright. All rights reserved.

Author Manuscript

enhancement in the operational lifetime of the Purcell-enhanced device, to yield T_{70} = 2900±100 h for an initial luminance of 1000 cd m^{-2}, compared to devices lacking this enhancement with T_{70} = 1000±100 h.

Introduction

Many attributes of phosphorescent organic light emitting diodes (PHOLEDs), such as a high internal quantum efficiency, wide color gamut, and accurate color rendering are desirable for both display and lighting applications[1–3]. Because white light is generated by exciting a combination of red, green, and blue emitting molecules, it is necessary for the lifetime of each element to be stable and importantly, comparable such that the color quality of the device does not noticeably change over its lifetime. Currently, both phosphorescent and fluorescent red and green OLEDs at L = 1000 cd m^{-2} can achieve commercially acceptable operational lifetimes of >180,000 h before reaching 70% of their initial luminance (T_{70})[3]. However, the lifetimes of blue phosphorescent emitters have lagged relative to their lower energy emitting red and green analogs, with light blue emitters demonstrating commercial operational lifetimes of 20,000 when aged at 1000 cd m^{-2} to T_{50} [3,4]. Previous studies have shown blue PHOLED lifetimes are limited by the generation of high energy excited states produced by triplet-triplet and triplet-polaron annihilation. These states have energies greater than the bond dissociation energies within the molecules, thus leading to molecular fragmentation[5,6]. For this reason, improved stability is achieved using less efficient fluorescent blue coupled with phosphorescent red and green emitters in white OLEDs (WOLEDs)[7–12]. To achieve all-phosphorescent WOLEDs it is necessary to compensate for the short blue emitter lifetime through the choice of materials and emission layer (EML) design, such as graded doping or hot excited state management[13,14]. Despite achieving high efficiencies while maintaining a high color rendering index (CRI), to our knowledge a color-stable

This article is protected by copyright. All rights reserved.

Author Manuscript

all phosphorescent WOLED has not yet been reported.[15–21] Recently, Zhao, et al. demonstrated the improvement of blue PHOLED operational lifetimes by more than a factor of four compared to conventional devices through the plasmon-exction-polariton (PEP)-enhanced Purcell effect. Here, PEPs result in an increase in Purcell factor, and improved coupling of energy from the EML to plasmonic modes on the metal cathode; both of which contribute to an enhancement in device lifetime[22].

The Purcell factor (*PF*) is defined as the cavity-enhanced triplet emission rate via $k_r = PF \cdot k_{r0}$, where k_{r0} is the natural triplet radiative rate. This phenomenon, known as the Purcell effect, is used to increase the radiative optical density of states within the PHOLED, thereby reducing the radiative lifetime of triplets. This, in turn, reduces their density within the EML, and thus the probability to produce high energy and damaging hot excited states. The Purcell effect is amplified by energy transfer to PEP modes formed at the interface between the electron-transporting layer (ETL) and the cathode. Coupling of plasmons in the Ag cathode adjacent to polaritons in the ETL significantly strengthens the Purcell effect compared to conventional PHOLEDs with an Al cathode. Previously, we demonstrated that the blue emissive element in a side-by-side WOLED degrades approximately 2.5 times faster to T_{70} than the red/green pixel operated at the same current density[23]. This suggests that the PEP-enhanced Purcell effect can stabilize the blue emission to the point where its lifetime is comparable to the red and green elements.

Here, we demonstrate an all phosphorescent stacked WOLED comprising a blue element adjacent to the cathode that is connected via a charge generation layer to a red/green emitting element, shown in Fig. 1a. We compare conventional devices employing an Al cathode (the control), to devices in which the radiative lifetime of the blue element is modified by PEPs through use of an Ag cathode (the Purcell-enhanced device) and an exciton-polariton coupling layer of BPyTP2. The BPyTP2 singlet emission spectrum overlaps with both the Ag plasmon absorption

This article is protected by copyright. All rights reserved.

Author Manuscript

while its absorption spectrum overlaps with the blue emission from the EML. The resulting strongly coupled polariton serves to decrease the triplet density in the EML by enhancing energy transfer from the EML to Ag plasmon modes. We achieve an initial external quantum efficiency of $EQE_{4\pi}$ = 19.1 ± 0.4% measured at 4π sr with a CRI = 76 and a correlated color temperature of CCT = 6100 K for the Purcell-enhanced device. This is compared with $EQE_{4\pi}$ = 13.0 ± 0.4% with CRI = 74 at 6900K for the control. We observe no measurable change in the colorimetric values for both devices at T_{70}, maintaining 1960 Commission Internationale de l'Eclairage (CIE) coordinates (*u*,*v*) = (0.17, 0.32) for the control and (0.18, 0.33) for the Purcell-enhanced devices. These latter WOLEDs exhibit an extrapolated T_{70} = 2900 ± 100 h at an initial luminance of 1000 cd m^{-2}, which is a 2.9 times improvement over the control device lifetime, as predicted by simulations[22]. By using the PEP-enhanced Purcell effect, we demonstrate a WOLED with CRI >75 that show a significant improvement in the stability of all color emission over the course of aging when compared to previously reported, summarized in Table S1.

Results

The stacked WOLED in Fig. 1a comprises two emissive layers, one red/green (R/G) and the other blue (B), separated by a charge generation layer (CGL). The control structure employs an Al, cathode, and the other a Purcell-enhanced, Ag, cathode. In both structures, BPyTP2 is used as the ETL. See Methods for IUPAC nomenclature for materials used. Overlap between the blue triplet and the BPyTP2 singlet exciton absorption spectra in Fig. S1, and the BPyTP2 emission and the Ag plasmon mode absorption enables efficient energy transfer to PEPs, as shown previously[22]. This is not observed in the control, where Al has only a weak plasmon resonance in the blue.

This article is protected by copyright. All rights reserved.

Author Manuscript

The coupling efficiencies into various available WOLED modes for photons emitted from the B and R/G elements calculated using Green's function methods are shown in Figs. 1b and c, respectively[24]. The distances of the B EML to the cathode, and the R/G EML to the CGL used in optimized devices are shown by dashed vertical lines. The calculated weighted average *PF* = 0.95 and 1.7 for the R/G and B layers within the control device, respectively, are compared with 0.91 and 2.2, respectively in the Purcell-enhanced device. Details on the calculation of the PF are included in Methods. The PF average, which depends on the position in the EML and the exciton concentration at each EML position, is weighted by the distribution of dopant throughout the EML. That is, dopant emission closer to the cathode has a higher PF than emission near the hole transport layer/EML interface. From Figs. 1b and c, there is a negligible change in the peak outcoupling efficiency between the control and Purcell-enhanced structures, from 16% to 17% for R/G, and no change for B. Coupling to plasmon modes is increased from 37% to 48% for B in the control and Purcell-enhanced devices, respectively.

The external quantum efficiencies in the forward viewing and 4π viewing directions are shown in Fig. 2a. We approximate the operating conditions of a white lighting fixture by accounting for emission from 4π sr and adding an external microlens array. Under these conditions, $EQE_{4\pi}$ = 12.8 ± 0.1% and 19.1 ± 0.3%, and $LPE_{4\pi}$ = 7.8 ± 0.1 lm/W and 10.8 ± 0.2 lm/W for control and Purcell-enhanced devices, respectively, corresponding to *L* =3300 +20 and 4330 ± 60 cd m^{-2}.

The *L-V* characteristics of the control and Purcell-enhanced devices are nearly identical, as shown in Fig. 2b. Similarly, there are no significant changes in the *J-V* characteristics between devices employing a Ag or Al cathode, whose turn on voltages are approximately 5.3 V. This is nearly double the voltage observed for single junction devices, since the B, with a turn on of 3 V, and R/G, with a turn on of 2.5 V, subelements are connected in series[23].

This article is protected by copyright. All rights reserved.

Author Manuscript

The emission spectra and spatial emission profiles both before and after aging at J = 10 mA cm^{-2}, are shown in Fig. 3a. The control and Purcell-enhanced devices cover 92% and 94% of the Lambertian profile, respectively, resulting in a shift in 1960 CIE (u, v) chromaticity coordinates of (Δu, Δv) = (0.04, 0.01) from viewing angles of 0º to 80º, as the effective cavity length decreases with increasing viewing angle[25]. The colorimetric coordinates, CRI, CCT, and the distances from the Planckian locus (Δuv) for the devices are provided in Table 1.

The devices were aged at J = 10 mA cm^2, corresponding to an initial luminance of $L_{0,4\pi}$ = 3300 ± 20 cd m^{-2} and 4330 ± 60 cd m^{-2} for control and Purcell-enhanced devices with results shown in Fig. 4. We obtain the times to reach 70% of their initial luminance of T_{70} = 1030 ± 20 h and 2900 ± 100 h, with a corresponding increase in voltage at a constant J of ΔV = 1.36 ± 0.03 and 1. 13 ± 0.01 V for the control and Purcell-enhanced devices, respectively.

At T_{70} there is no measurable change in device (u, v) chromaticity coordinates and CRI for either device, although the control electroluminescence spectrum exhibits a small change in wavelength dependence with aging corresponding to a red shift in CCT, ΔCCT = 100K, while there is no measurable wavelength or CCT shift for the Purcell-enhanced device (see Fig 3a). The wavelength changes are characterized by fitting the white spectrum to the sum of the individual spectra of the separate red, green, and blue emitting materials provided in Fig. 3b, corresponding to three peaks from Ir(dmp)$_3$ and Ir(ppy)$_3$, and two from PQIr. A representative fit for the Purcell enhanced device is shown inset of Fig. 3b, with a summary of all fit parameters found in Table 2. Using these fits, we can determine the change in spectra from their differences also shown in Fig. 3b. The Purcell-enhanced devices shows a nearly uniform, <6% change in peak magnitude across all wavelengths, while the control exhibits a 47% decrease in the 524 nm vibronic of Ir(dmp)$_3$, and a >8% change across red and green.

The lifetime is normalized to an initial luminance of L_0 = 1000 cd m^{-2} using[3]:

This article is protected by copyright. All rights reserved.

Author Manuscript

$$T_X(L_0) = T_X(L_{0,test})\left({L_{0,test}}/{L_0}\right)^n \quad \textbf{(1)}$$

where T_X is the device lifetime at a fraction, x, of the initial luminance. The acceleration factor, n = 1.3 ± 0.1 for the control and n = 1.5 ± 0.1 for the Purcell-enhanced device is found by solving Eq. 1 using the lifetime and initial luminance of devices aged at J = 5 mA cm^{-2} and J = 10 mA cm^{-2}, with data compiled in Table **3**. We find that for L_0 = 1000 cd m^{-2}, the operational lifetime is T_{70} = 1030 ± 40 h for the control and 2900 ± 60 h for the Purcell-enhanced devices, demonstrating a 2.9 times enhancement. Raw data for devices aged at equivalent current densities before normalizing to constant luminance are shown in Fig. S2.

Discussion

The device stack in Fig. 1a employs a 17 nm thick BPyTP2 ETL to optimize coupling between the blue EML and plasmonic modes formed on the metal cathode surface, and outcoupling to air modes of emission from both the B and R/G EMLs. A thinner ETL suppresses outcoupling to air modes as shown in Fig. 1b, while a thicker ETL decreases coupling to the SPP modes formed at the control ETL/Al interface and PEP modes at the ETL/Ag interface[22]. The outcoupling efficiency of the R/G element is optimized for a 100 nm thick ETL; in this work, we use a thickness of 60 nm, which is sufficient to provide outcoupling efficiencies of approximately 17% for both the Purcell-enhanced and control devices, with 20% for the blue element, and is sufficiently thin to assure a low operating voltage. Additional fresh data for a device with an 80nm thick R/G ETL is shown in Table S2 and Fig. S3, which demonstrates a red shift in its spectrum because of the increased ETL thickness. The red shift with thicker R/G ETL is the result of higher coupling to air modes from the R/G layer, shown in Fig. 1c. However, there is no significant difference in the electrical performance between 60 and 80 nm ETL devices, indicating the charge balance is better for the device with the thinner ETL. The cathode/ETL structure is optimized for the B element. Because R/G emission is generated far from the cathode, the dependence of R/G

This article is protected by copyright. All rights reserved.

Author Manuscript

outcoupling on B ETL thickness, shown in Fig. S4, varies by only ~7% across a 15 nm range of B ETL thicknesses, which is less than half the observed change in plasmon coupling for emission from the B EML across the same range. Thus, the choice of B ETL thickness can be optimized independent of the R/G subelement. In the blue EML, the Purcell-enhanced structure increases *PF* by a factor of 1.4 relative to the control.

The CGL between the B and R/G elements enables each injected electron to generate two photons. The measured forward direction EQE = 12.2%, therefore, is low due to the relatively low quantum efficiencies of both the B and R/G emitting sections. That is, the blue discrete blue-emitting $Ir(dmp)_3$ devices have EQE = 9.5%, and R/G devices have EQE = 12%.[13,23] Indeed, conventional WOLEDs used in lighting have up to 5 or 6 emitting sections to achieve high efficiency and brightness. Nevertheless, this relatively simple archetype device achieves CRI = 76 at a high color temperature of CCT = 6100 due to strong blue emission, that is unchanged over the course of aging. The chromaticity coordinates have a minimal viewing angle dependence, showing a slight blue shift from a viewing angle of 0º to 80º. The corresponding change in the distance from the *u,v* coordinates to the closest point on the Planckian locus, Δ*uv*, shifts δΔ*uv* = -0.033 for the control and -0.035 for the Purcell-enhanced devices, where δΔ*uv* is defined as the change in Δ*uv* corresponding to a viewing angle shift from 0º to 80º.[23]

Stability of the blue emission is due to the reduced radiative lifetime resulting from coupling between the triplets and SPP modes in the control device. In comparison, previously demonstrated long-lived stacked WOLEDs have shown noticeable red shifts at T_{70}, corresponding to a 50% decrease in luminance from the blue, despite the use of triplet managers to extend the blue emitter lifetime[18]. In work that utilizes the same EML structures in a side-by-side rather than stacked geometry, a red shift of (Δ*u*,Δ*v*) = (0.014,−0.002) is observed, while here (Δ*u*,Δ*v*) = (0.002, 0.000) falls within the margin of error[23]. This demonstrates a significant improvement over previous WOLEDs with both phosphorescent and fluorescent blue emitters

This article is protected by copyright. All rights reserved.

Author Manuscript

for which either (Δu,Δv) is 10× greater or color stability has not been reported.[10–12,15–21,26–29] A summary of reported WOLED data in the literature is included in Table S1**.** In the Purcell-enhanced device, blue triplets are strongly coupled to PEP modes, resulting in improved spectral stability (cf. Fig. 3a) along with a significant increase in lifetime. Use of the PEP-enhanced Purcell effect results in a reduction in the voltage rise over the course of aging by 0.23V compared to the control, and a 2.9 times increase in T_{70}. This operational lifetime enhancement is in agreement with the 2.9 times enhancement expected at T_{70} based on the power law, m = 1.7 ± 0.1, dependence between PF and operational lifetime (i.e. $T_x \sim PF^m$), as previously reported[22].

Conclusion

We demonstrated a single stacked white-emitting PHOLED with improved operational lifetime due to exciton-plasmon-polariton coupling that increases the optical density of states within the OLED cavity of the blue subelement. This, in turn, decreases the blue triplet lifetime, thereby reducing the probability for generating high energy excited states via triplet annihilation processes that lead to molecular dissociation. We observe no change in emission color across the entire white spectrum for Purcell-enhanced devices, demonstrating that the polariton-enhanced Purcell effect improves B subelement lifetime such that it degrades at the same rate as the R/G subelement. While this work demonstrates a relatively simple device design with a high CRI and operational stability, the color quality and lifetime can be further improved by increasing the strength of the Purcell effect with a sub-anode reflector and increasing EQE using more efficient blue phosphorescent material. Furthermore, high brightness and efficient stacked PHOLEDs typically are comprised of at least 3 – 5 R/G elements to improve both lifetime and CRI[18]. The design introduced here only affects the single blue emitting subelement in the stack

This article is protected by copyright. All rights reserved.

Author Manuscript

near the cathode, and hence does not preclude the addition of more R/G elements to achieve practical long-lived, bright, and color-balanced emission.

Methods

Device Fabrication: Prior to organic layer deposition, pre-patterned ITO anodes (15 Ω/sq) on glass substrates (Lumtec) are sonicated in detergent, deionized water, acetone (x2), isopropanol (165ºC, x2), and dried using pure N_2. The 2 mm^2 device is defined by the 1 mm width of the ITO stripes and the 2 mm width of the shadow mask placed perpendicular to the ITO used for cathode metal patterning.

Vacuum thermal evaporation is used to deposit the organic layers. As shown in Fig. 1a, the layers comprise 10 nm thick hexaazatriphenylene hexacarbonitrile (HATCN, Universal Display Corp., UDC), 30 nm thick N,N'-di(1-naphthyl)-N,N'-diphenyl-(1,1'-biphenyl)-4,4'-diamine (NPD, UDC), 12 nm thick 10%vol bis(2-phenylquinolyl-N,$C^{2'}$) acetylacetonate iridium(III) (PQIr, UDC) doped into 4,40-bis(3-methylcarbazol-9-yl)-2,20-biphenyl (mCBP, UDC), 12 nm thick 8%vol tris[2-phenylpyridinato-C^2,N]iridium(III) ($Ir(ppy)_3$, Lumtec) doped into mCBP, 5 nm thick Bis(8-hydroxy-2-methylquinoline)-(4-phenylphenoxy)aluminum (BAlq, Universal Display Corp.), 10 nm thick 10%vol PQIr:mCBP, 60 nm thick 2,7-bis(2,20-bipyridine-5-yl)triphenylene (BPyTP2, Lumtec), 12 nm thick 1:1 mol BPyTP2:Li (Kurt J. Lesker), 12 nm thick HATCN, 15 nm thick NPD, 50 nm thick 18 to 8%vol tris[3-(2,6-dimethylphenyl)-7-methylimidazo[1,2-f] phenanthridine] iridium(III) ($Ir(dmp)_3$:mCBP, UDC), 5 nm thick mCBP, 17nm BPyTP2, and 1.5 nm thick Li quinolate (Liq, Lumtec). Control devices have a 100 nm thick Al (Alfa Azar) cathode, and Purcell-enhanced devices have a 120 nm thick Ag (Sigma Aldrich) cathode. Organic materials from Lumtec are purified via thermal gradient sublimation.[30] The devices are encapsulated in ultrapure N_2 with glass cover slide attached using UV-curing epoxy (Epotek).

This article is protected by copyright. All rights reserved.

Author Manuscript

Device modeling, characterization, lifetime testing: The forward, 2π, J-V-L characteristics are measured using a parameter analyzer (Keysight) and a large area Si photodetector (Hamamatsu). The 4π measurements use an integrating sphere with a commercial external microlens array (Lumtec). Error reported is the standard deviation from a population of four devices. Electroluminescence and angle-dependent spectra are measured via fiber coupling to a spectrometer (Ocean Optics). Device spectra are fit to Gaussian functions using MATLAB. The devices are aged under constant current, supplied by a source-measuring unit (Agilent), and device luminance is measured at 1-3 min intervals using a photodiode. The coupling efficiencies are calculated using Green's function methods[24]. Following the work of Celebi, et al., we use the Chance, Prock, and Sibley model to describe the electric field of an emissive dipole using dyadic Green's functions in the stacked structure shown in Fig. 1a. The layer thicknesses and complex indexes of refraction are measured by ellipsometry (J.A. Woollam). From the model, we compute the ratio of the decay rate for vertical and horizontal dipoles, $b_{||}$ and $b_{\perp}$, to the natural decay rate, b_0 , in vacuum:

$$\frac{b_{||}}{b_0} = 1 - q + q\left\{1 + \frac{3}{4}\mathrm{Re}\left[\int_0^\infty d\kappa \frac{\kappa}{h_s k_s}\left(c_s + c_s' + \frac{{h_s}^2}{{k_s}^2}(f_s - f_s')\right)\right]\right\} \quad \textbf{(2)}$$

and $$\frac{b_{\perp}}{b_0} = 1 - q + q\left\{1 + \frac{3}{2}\mathrm{Re}\left[\int_0^\infty d\kappa \frac{\kappa^3}{h_s k_s^3}(f_s + f_s')\right]\right\}, \quad \textbf{(3)}$$

where q is the quantum yield of the emitter, κ and h are the parallel and perpendicular amplitudes of the propagation vector k, f and c, and f' and c' are left and right travelling wave coefficients of the Green's functions used to describe the dipole source, and the subscript s is the index of the dipole emitting layer. Because the PF is equivalent to the total decay rate, then:

$$PF = b_{tot} = \theta_{hor}\frac{b_{||}}{b_0} + (1 - \theta_{hor})\frac{b_{\perp}}{b_0}, \quad \textbf{(4)}$$

This article is protected by copyright. All rights reserved.

Author Manuscript

where θ_{hor} is the horizontal dipole fraction. PF is calculated with 1 nm resolution throughout the EML, and the average PF is weighted by the doping concentration across each EML. We assume that the exciton concentration is proportional to the dopant concentration[13]. We assume θ_{hor} = 0.77 and q = 0.45 for the B EML and q = 0.95 for the R/G EML. The peak emissive wavelengths of λ = 600 nm and λ = 475 nm are used for the R/G and B EML calculations, respectively.

Funding Sources

The authors acknowledge Universal Display Corporation and the U.S. Department of Energy's Office of Energy Efficiency and Renewable Energy (EERE) under the Award Number DE-EE0009688. This report was prepared as an account of work sponsored by an agency of the United States Government. Neither the United States Government nor any agency thereof, nor any of their employees, makes any warranty, express or implied, or assumes any legal liability or responsibility for the accuracy, completeness, or usefulness of any information, apparatus, product, or process disclosed, or represents that its use would not infringe privately owned rights. Reference herein to any specific commercial product, process, or service by trade name, trademark, manufacturer, or otherwise does not necessarily constitute or imply its endorsement, recommendation, or favoring by the United States Government or any agency thereof. The views and opinions of authors expressed herein do not necessarily state or reflect those of the United States Government or any agency thereof.

Author Contributions

This article is protected by copyright. All rights reserved.

Author Manuscript

C.E.A fabricated and measured all devices. C.E.A. and H.Z. designed the devices. C.E.A., H.Z., and S.R.F. analyzed the data, and S.R.F. supervised the project. The manuscript was written by C.E.A. and S.R.F. and edited by all co-authors.

Data Availability

The data that support the findings of this study are available from the corresponding author upon reasonable request.

Competing Interests

One of the authors (SRF) has an equity interest in Universal Display Corporation (UDC). This conflict of interest in under management by the University of Michigan's Office of the Vice President for Research. The University of Michigan has a license agreement with UDC.

This article is protected by copyright. All rights reserved.

Author Manuscript

References

(1) So, F.; Kido, J.; Burrows, P. Organic Light-Emitting Devices for Solid-State Lighting. *MRS Bull.* **2008**, *33*, 663–669.

(2) Wu, Z.; Ma, D. Recent Advances in White Organic Light-Emitting Diodes. *Mater. Sci. Eng. R Rep.* **2016**, *107*. https://doi.org/10.1016/j.mser.2016.06.001.

(3) Forrest, S. R. *Organic Electronics: Foundations to Applications*; Oxford University Press, USA, 2020.

(4) Adachi, C.; Baldo, M. A.; Thompson, M. E.; Forrest, S. R. Nearly 100% Internal Phosphorescence Efficiency in an Organic Light Emitting Device. *J. Appl. Phys.* **2001**, *90* (10), 5048–5051. https://doi.org/10.1063/1.1409582.

(5) Giebink, N. C.; D'Andrade, B. W.; Weaver, M. S.; MacKenzie, P. B.; Brown, J. J.; Thompson, M. E.; Forrest, S. R. Intrinsic Luminance Loss in Phosphorescent Small-Molecule Organic Light Emitting Devices Due to Bimolecular Annihilation Reactions. *J. Appl. Phys.* **2008**, *103* (4). https://doi.org/10.1063/1.2884530.

(6) Jeong, C.; Coburn, C.; Idris, M.; Li, Y.; Djurovich, P. I.; Thompson, M. E.; Forrest, S. R. Understanding Molecular Fragmentation in Blue Phosphorescent Organic Light-Emitting Devices. *Org. Electron.* **2019**, *64*, 15–21. https://doi.org/10.1016/j.orgel.2018.10.001.

(7) Birnstock, J.; He, G.; Murano, S.; Werner, A.; Zeika, O. 54.3: White Stacked OLED with 35 Lm/W and 100,000 Hours Lifetime at 1000 Cd/m ^{2} for Display and Lighting Applications. *SID Symp. Dig. Tech. Pap.* **2008**, *39* (1), 822–825. https://doi.org/10.1889/1.3069797.

(8) Hatwar, T. K.; Spindler, J. P.; Kondakova, M.; Giesen, D.; Deaton, J.; Vargas, J. R. 52.2: Hybrid Tandem White OLEDs with High Efficiency and Long Life-time for AMOLED Displays

This article is protected by copyright. All rights reserved.

Author Manuscript

and Solid-State Lighting. *SID Symp. Dig. Tech. Pap.* **2010**, *41* (1), 778–781. https://doi.org/10.1889/1.3500587.

(9) Kanno, H.; Giebink, N. C.; Sun, Y.; Forrest, S. R. Stacked White Organic Light-Emitting Devices Based on a Combination of Fluorescent and Phosphorescent Emitters. *Appl. Phys. Lett.* **2006**, *89* (2). https://doi.org/10.1063/1.2219725.

(10) Chen, Y.; Yang, D.; Qiao, X.; Dai, Y.; Sun, Q.; Ma, D. Novel Strategy to Improve the Efficiency Roll-off at High Luminance and Operational Lifetime of Hybrid White OLEDs *via* Employing an Assistant Layer with Triplet–Triplet Annihilation up-Conversion Characteristics. *J. Mater. Chem. C* **2020**, *8* (19), 6577–6586. https://doi.org/10.1039/D0TC00867B.

(11) Huang, C.; Zhang, Y.; Zhou, J.; Sun, S.; Luo, W.; He, W.; Wang, J.; Shi, X.; Fung, M. Hybrid Tandem White OLED with Long Lifetime and 150 Lm W^{-1} in Luminous Efficacy Based on TADF Blue Emitter Stabilized with Phosphorescent Red Emitter. *Adv. Opt. Mater.* **2020**, *8* (18), 2000727. https://doi.org/10.1002/adom.202000727.

(12) Liu, F.; Liu, H.; Tang, X.; Ren, S.; He, X.; Li, J.; Du, C.; Feng, Z.; Lu, P. Novel Blue Fluorescent Materials for High-Performance Nondoped Blue OLEDs and Hybrid Pure White OLEDs with Ultrahigh Color Rendering Index. *Nano Energy* **2020**, *68*, 104325. https://doi.org/10.1016/j.nanoen.2019.104325.

(13) Zhang, Y.; Lee, J.; Forrest, S. R. Tenfold Increase in the Lifetime of Blue Phosphorescent Organic Light-Emitting Diodes. *Nat. Commun.* **2014**, *5*. https://doi.org/10.1038/ncomms6008.

(14) Lee, J.; Jeong, C.; Batagoda, T.; Coburn, C.; Thompson, M. E.; Forrest, S. R. Hot Excited State Management for Long-Lived Blue Phosphorescent Organic Light-Emitting Diodes. *Nat. Commun.* **2017**, *8*. https://doi.org/10.1038/ncomms15566.

This article is protected by copyright. All rights reserved.

Author Manuscript

(15) Reineke, S.; Lindner, F.; Schwartz, G.; Seidler, N.; Walzer, K.; Lüssem, B.; Leo, K. White Organic Light-Emitting Diodes with Fluorescent Tube Efficiency. *Nature* **2009**, *459* (7244). https://doi.org/10.1038/nature08003.

(16) Ou, Q.; Zhou, L.; Li, Y.; Shen, S.; Chen, J.; Li, C.; Wang, Q.; Lee, S.; Tang, J. Extremely Efficient White Organic Light-Emitting Diodes for General Lighting. *Adv. Funct. Mater.* **2014**, *24* (46), 7249–7256. https://doi.org/10.1002/adfm.201402026.

(17) Wu, S.; Li, S.; Wang, Y.; Huang, C.; Sun, Q.; Liang, J.; Liao, L.; Fung, M. White Organic LED with a Luminous Efficacy Exceeding 100 Lm W^{-1} without Light Out-Coupling Enhancement Techniques. *Adv. Funct. Mater.* **2017**, *27* (31), 1701314. https://doi.org/10.1002/adfm.201701314.

(18) Coburn, C.; Jeong, C.; Forrest, S. R. Reliable, All-Phosphorescent Stacked White Organic Light Emitting Devices with a High Color Rendering Index. *ACS Photonics* **2018**, *5* (2). https://doi.org/10.1021/acsphotonics.7b01213.

(19) Jeon, S.; Lee, S.; Han, K.; Shin, H.; Kim, K.; Jeong, J.; Kim, J. High-Quality White OLEDs with Comparable Efficiencies to LEDs. *Adv. Opt. Mater.* **2018**, *6* (8), 1701349. https://doi.org/10.1002/adom.201701349.

(20) Yu, H.; Dai, X.; Yao, F.; Wei, X.; Cao, J.; Jhun, C. Efficient White Phosphorescent Organic Light-Emitting Diodes Using Ultrathin Emissive Layers (<1 Nm). *Sci. Rep.* **2018**, *8* (1), 6068. https://doi.org/10.1038/s41598-018-24434-8.

(21) Ameri, L.; Cao, L.; Tan, X.; Li, J. Efficient, Color-Stable, and Long-Lived White Organic Light-Emitting Diodes Utilizing Phosphorescent Molecular Aggregates. *Adv. Mater.* **2023**, *35* (11), 2208361. https://doi.org/10.1002/adma.202208361.

This article is protected by copyright. All rights reserved.

Author Manuscript

(22) Zhao, H.; Arneson, C. E.; Fan, D.; Forrest, S. R. Stable Blue Phosphorescent Organic LEDs That Use Polariton-Enhanced Purcell Effects. *Nature* **2024**, *626* (7998), 300–305. https://doi.org/10.1038/s41586-023-06976-8.

(23) Arneson, C.; Huang, X.; Forrest, S. R. Solid-State Lighting Using Side-by-Side White Phosphorescent Organic Light-Emitting Diodes. *ACS Photonics* **2023**, *10* (2), 526–533. https://doi.org/10.1021/acsphotonics.2c01698.

(24) Celebi, K.; Heidel, T. D.; Baldo, M. A. Simplified Calculation of Dipole Energy Transport in a Multilayer Stack Using Dyadic Green's Functions. *Opt. Express* **2007**, *15* (4), 1762. https://doi.org/10.1364/OE.15.001762.

(25) Bulović, V.; Khalfin, V.; Gu, G.; Burrows, P.; Garbuzov, D. Weak Microcavity Effects in Organic Light-Emitting Devices. *Phys. Rev. B - Condens. Matter Mater. Phys.* **1998**, *58* (7). https://doi.org/10.1103/PhysRevB.58.3730.

(26) Zhu, L.; Zhao, Y.; Zhang, H.; Chen, J.; Ma, D. Using an Ultra-Thin Non-Doped Orange Emission Layer to Realize High Efficiency White Organic Light-Emitting Diodes with Low Efficiency Roll-Off. *J. Appl. Phys.* **2014**, *115* (24), 244512. https://doi.org/10.1063/1.4886179.

(27) Yao, J.; Liu, W.; Lin, C.; Sun, Q.; Dai, Y.; Qiao, X.; Yang, D.; Chen, J.; Ma, D. High Efficiency and Long Lifetime Fluorescent White Organic Light-Emitting Diodes by Phosphor Sensitization to Strategically Manage Singlet and Triplet Excitons. *J. Mater. Chem. C* **2021**, *9* (10), 3626–3634. https://doi.org/10.1039/D1TC00113B.

(28) Zhang, C.; Lu, Y.; Liu, Z.; Zhang, Y.; Wang, X.; Zhang, D.; Duan, L. A π–D and π–A Exciplex-Forming Host for High-Efficiency and Long-Lifetime Single-Emissive-Layer Fluorescent

This article is protected by copyright. All rights reserved.

Author Manuscript

White Organic Light-Emitting Diodes. *Adv. Mater.* **2020**, *32* (42), 2004040. https://doi.org/10.1002/adma.202004040.

(29) Wang, Z.; Li, X.; Ma, Z.; Cai, X.; Cai, C.; Su, S. Exciton-Adjustable Interlayers for High Efficiency, Low Efficiency Roll-Off, and Lifetime Improved Warm White Organic Light-Emitting Diodes (WOLEDs) Based on a Delayed Fluorescence Assistant Host. *Adv. Funct. Mater.* **2018**, *28* (11), 1706922. https://doi.org/10.1002/adfm.201706922.

(30) Forrest, S. R. Ultrathin Organic Films Grown by Organic Molecular Beam Deposition and Related Techniques. *Chem. Rev.* **1997**, *97* (6), 1793–1896. https://doi.org/10.1021/cr941014o.

Tables

Table 1 – As-prepared Device Colorimetric Parameters

	1960 CIE (u, v)	CRI	CCT (K)	Δuv
Control	(0.17, 0.32)	74	6900	0.031
Purcell-enhanced	(0.18, 0.33)	76	6100	0.025

Table 2 – Spectral Parameters

		Normalized Peak Height					
		Purcell-enhanced			**Control**		
		Fresh	**T_{70}**	**Δ%***	**Fresh**	**T_{70}**	**Δ%**
	R-sqared value	0.9988	0.9987		0.9982	0.9979	
	RMS Error	0.01	0.01		0.01	0.01	
Dopant	**Center wavelength (nm)**						
Ir(dmp)3	465	0.73	0.72	-1.2	0.70	0.70	-1.2

This article is protected by copyright. All rights reserved.

Author Manuscript

	491	0.55	0.55	-1.2	0.54	0.53	-1.2
	524	0.25	0.24	-5.4	0.20	0.10	-47.5
Ir(ppy)3	513	0.16	0.17	5.9	0.16	0.19	17.9
	543	0.21	0.22	5.9	0.21	0.25	17.9
	584	0.32	0.32	1.4	0.29	0.31	8.5
PQIr	631	0.21	0.22	3.4	0.17	0.15	-10.9
	596	0.23	0.24	3.4	0.18	0.16	-10.9

* Δ% is defined as the percent change in peak intensity from the fresh to T_{70} fit

Table 3 – Lifetime and Aging Parameters

	5 mA cm^{-2}			**10 mA cm^{-2}**							
	L_0 (cd m^{-2})	**L_0 * (cd m^{-2})**	**T_{90} (h)**	**L_0 (cd m^{-2})**	**L_0 * (cd m^{-2})**	**T_{90} (h)**	**T_{70} (h)**	**PF**	**n**	**T_{70} $^{+}$ (h)**	**T_{70} $^{+,*}$ (h)**
Control	1120	1550	73	2240	3300	29	219	1.6	1.3	640	1030
Purcell-enhanced	1389	2270	125	2940	4330	41	325	2.2	1.5	1600	2940

* Measured using an external microlens array and integrating sphere

$^{+}$ Normalized to L_0 = 1000 cd m^{-2}

Figure Captions

This article is protected by copyright. All rights reserved.

Author Manuscript

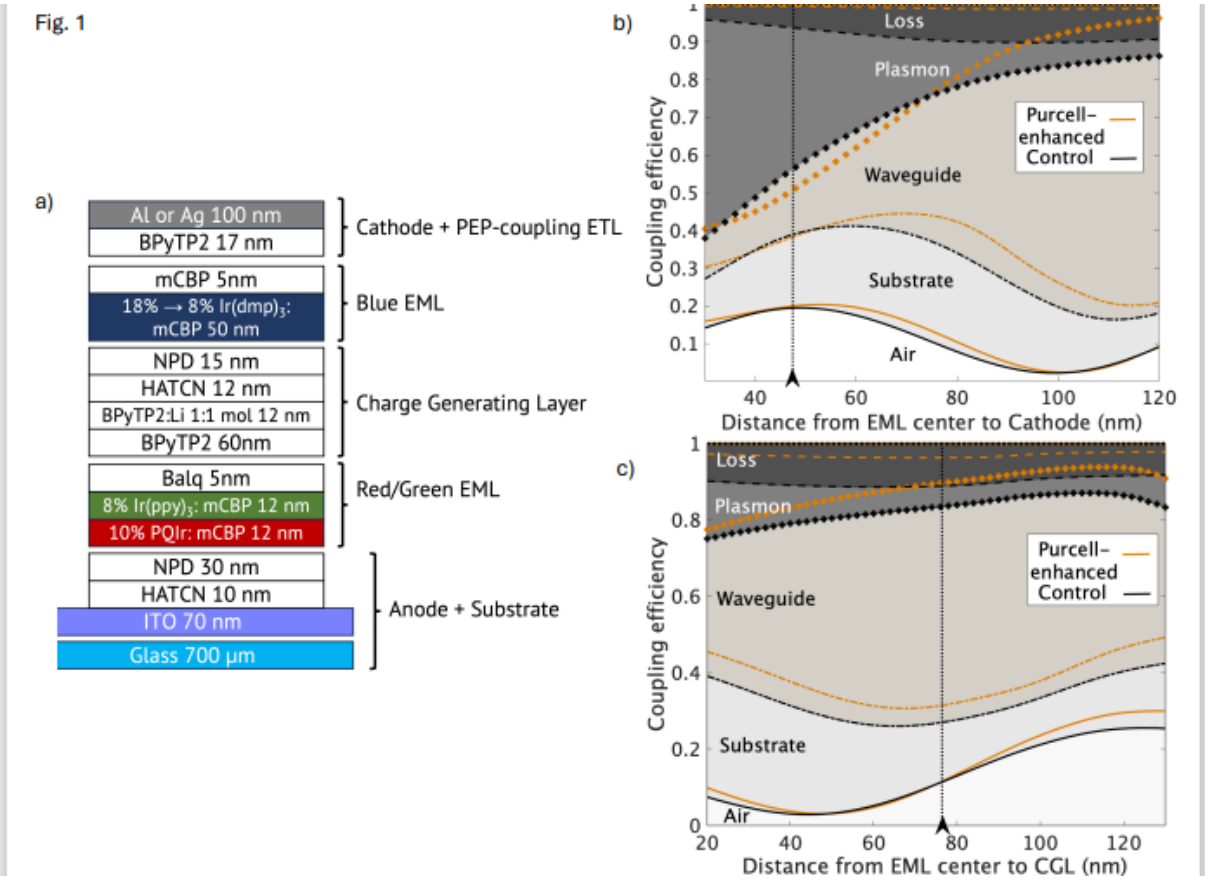


Figure 1. a) Schematic illustration of the device structure. Coupling efficiencies to lossy, surface plasmon polariton, organic waveguide, substrate, and air modes are calculated using Green's function methods for the blue, b), and red/green, c), elements for the control device are indicated by the shaded areas and black lines, and Purcell-enhanced structures are indicated by the orange lines**.** The horizontal axis shows the results for various spacings between the blue EML and the cathode, b), and the red/green EML and the CGL, c). The dotted vertical lines correspond to the structures used in this work. The vertical axis shows the fractional coupling efficiency into each mode, where the total of all modes is equivalent to 1. The fraction of coupling to each mode can be found by the vertical distance between black lines for the control, and orange lines for the Purcell-enhanced structure.

This article is protected by copyright. All rights reserved.

Author Manuscript

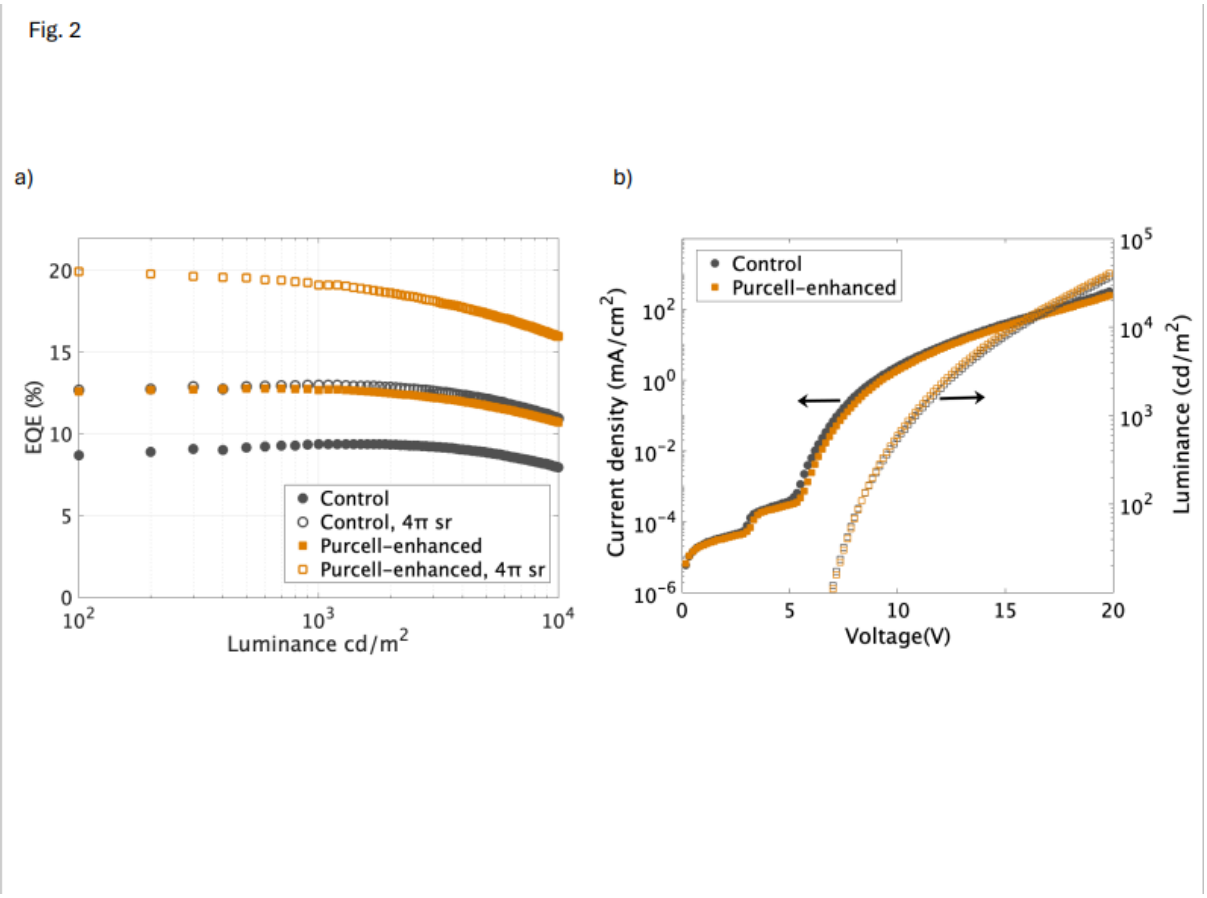


Figure 2. a) Device external quantum efficiency for forward viewing in 2π solid angle (filled symbols) and 4π solid angle with an external microlens array (open symbols) as a function of brightness. b) Current-voltage-luminance characteristics of the control and Purcell-enhanced devices.

This article is protected by copyright. All rights reserved.

Author Manuscript

Fig. 3

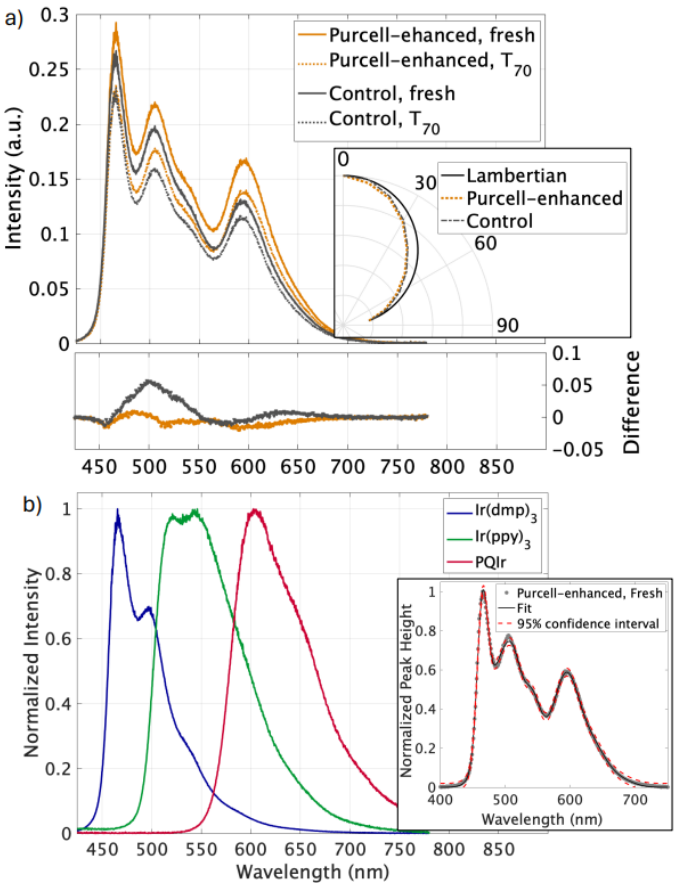


Figure 3. a) Device spectra measured at normal incidence for both control and Purcell-enhanced devices before aging (fresh) and at T_{70}. The differences between normalized spectra for control and Purcell-enhanced devices are indicated on the right axis of the lower plot. *Inset*: Angular device emission profile. A Lambertian profile is indicated by the black line for reference. b) Individual spectra for $Ir(dmp)_3$ (blue), $Ir(ppy)_3$ (green), and PQIr (red) phosphors in thin films. *Inset*: Fitting using the individual spectra for the fresh, white emitting Purcell-enhanced device.

This article is protected by copyright. All rights reserved.

Author Manuscript

Fig. 4

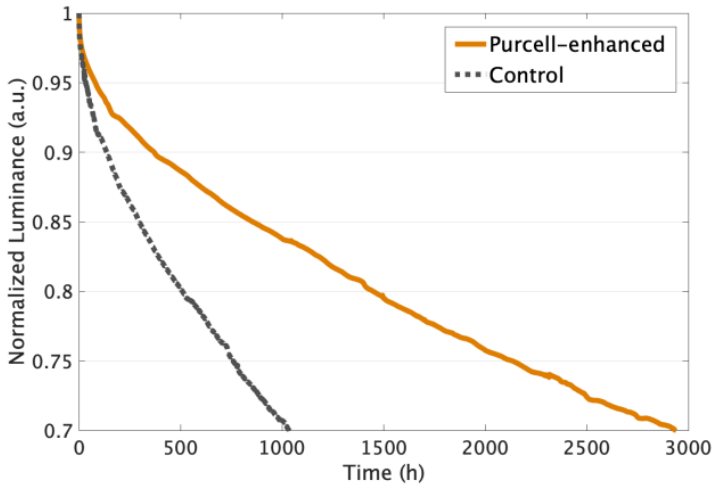
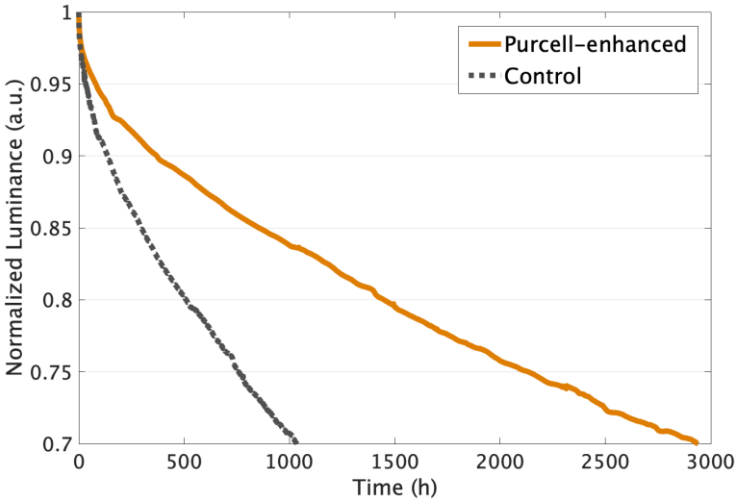


Figure 4. Change in luminance vs. time for control and Purcell-enhanced devices, normalized to aging at an initial luminance of 1000 cd m^{-2}.

The operational lifetime and color stability of a stacked white emitting all-phosphorescent OLEDs has been significantly improved through utilization of the plasmon-exciton-polariton-enhanced (PEP) Purcell effect to extend the life of the blue phosphorescent sub-element such that it ages at the same rate as the green and red phosphorescent elements.

This article is protected by copyright. All rights reserved.

Author Manuscript



This article is protected by copyright. All rights reserved.